

Modeling and Experimental Validation of Electrochemical Reduction of CO₂ to CO in a Microfluidic Cell

To cite this article: Kunna Wu *et al* 2015 *J. Electrochem. Soc.* **162** F23

View the [article online](#) for updates and enhancements.



*Benefit from connecting
with your community*

ECS Membership = Connection

ECS membership connects you to the electrochemical community:

- Facilitate your research and discovery through ECS meetings which convene scientists from around the world;
- Access professional support through your lifetime career;
- Open up mentorship opportunities across the stages of your career;
- Build relationships that nurture partnership, teamwork—and success!

Join ECS! **Visit electrochem.org/join**





Modeling and Experimental Validation of Electrochemical Reduction of CO₂ to CO in a Microfluidic Cell

Kunna Wu,^{a,b} Erik Birgersson,^{a,*} Byoungsu Kim,^b Paul J. A. Kenis,^{b,*} and Iftekhar A. Karimi^{a,z}

^aDepartment of Chemical and Biomolecular Engineering, National University of Singapore, Singapore 117585

^bDepartment of Chemical and Biomolecular Engineering, University of Illinois at Urbana-Champaign, Urbana, Illinois 61801, USA

A steady-state isothermal model is presented for the electrochemical reduction of CO₂ to CO in a microfluidic flow cell. The full cell model integrates the transport of charge, mass, and momentum with electrochemistry for both the cathode and anode. Polarization curves obtained from experiments conducted at different flow rates with varying applied cell potentials are used to determine the kinetic parameters in the electrochemical reaction rate equations. The parameterized model is validated using a different set of experimental results. Good agreement is observed, especially at high cell potentials (−2.5 to −3 V). The model is further used to analyze the effects of several operating parameters, such as applied cell potential, CO₂ concentration of the feed and feed flow rates. The use of the model to analyze the effect of design parameters, such as channel length and porosity of the gas diffusion electrodes, is also demonstrated.

© 2014 The Electrochemical Society. [DOI: 10.1149/2.1021414jes] All rights reserved.

Manuscript submitted July 2, 2014; revised manuscript received October 9, 2014. Published November 4, 2014.

Global CO₂ emissions from the combustion of fossil fuels have increased by about 60% between 1990 (the Kyoto Protocol reference year) and 2013, with approximately 9.9 GtC added to the atmosphere in 2013.¹ Several studies indicate that CO₂ emissions must be reduced significantly, by as much as 50% of those in 1990, by 2050 to limit the potential effects of climate change.^{2–5} Utilizing captured CO₂ as a feedstock for the production of useful products is increasingly being explored as an alternative to geological sequestration. Considerable research is underway in several directions to advance the promise of processes that utilize CO₂. Essentially, three pathways exist for utilizing CO₂: (1) convert it into fuels; (2) utilize it as a feedstock for chemicals; or (3) use it as a solvent, working fluid, or heat transfer fluid.⁶

Electrochemical conversion of CO₂ into useful products with the help of a renewable or carbon neutral electricity source, such as solar, wind, or hydro power, also is receiving increased attention, as it can serve as a mechanism for storing excess energy from intermittent renewable sources as fuels.⁷ Several electrochemical flow reactor designs have been reported in the literature, such as an electrolytic cell with a separator,⁸ solid oxide electrolysis cells,^{9–12} and microfluidic electrolytic cells.^{13–15} In these reactors, CO₂ is fed into the reactor at the cathode side and reduced to chemicals such as carbon monoxide (CO),^{8,16–18} formic acid/formate (HCOOH/HCOO[−]),^{13,19–21} methane,^{22–24} ethylene,^{25–29} and alcohols.^{30–32} The product selectivity depends on the cathode catalyst, applied potential, and the electrolyte composition. A variety of catalysts, including various metals,^{21,33–35} metal oxides,³⁶ metal organic frameworks,³⁷ and organometallic compounds³⁸ have been tested. For recent developments in reactor design, catalyst selection, and electrode structure for the electrochemical reduction of CO₂, the reader is referred to the review articles by Jhong et al.³⁹ and Lim et al.⁴⁰

The majority of studies on the electrochemical conversion of CO₂ have been experimental in nature. They have explored different types of electrodes and catalysts to improve performance, and to unravel the possible electro-reduction mechanisms.^{39–41} First-principles modeling of electrochemical reactors can complement the experimental work reported to date by elucidating the complex interplay between transport and electrochemistry, particularly in porous electrodes. The results of such studies can help in the design and optimization of these electrochemical reactors. Previously, Li & Oloman presented a crude cathode model for the electro-reduction of CO₂ to potassium formate in a continuous “trickle-bed” reactor.⁴² However, the agreement between the

numerical and experimental results was poor. Delacourt & Newman proposed a detailed model for the reduction of CO₂ to CO in a cell similar to a proton-exchange-membrane fuel cell, but with an additional aqueous buffer layer.⁴³ Their model predicted the experimental data pretty well, but only at current densities smaller than 10 mA/cm². Several models have also been developed for the electro-reduction of CO₂ in a solid oxide electrolyzer cell (SOEC).^{44–47} However, for microfluidic flow cells (MFCs), which have been demonstrated in several experimental studies^{13–15,38} to be an effective reactor and a versatile analytical tool for the electro-reduction of CO₂, not much modeling work has been reported in literature. Wang and his coworkers⁴⁸ first developed a model for CO₂ electro-reduction to aqueous formate solution in such a MFC. Instead of aqueous formate, we will consider the electrochemical reduction of CO₂ to gaseous CO, which has not been studied in the literature. The difference in the products, and thus reaction mechanisms, leads to different treatments of the electrochemical reaction kinetics. We consider CO formation, as CO can be combined with H₂ to yield syngas, which can be converted into fuels in the Fischer-Tropsch process.^{49–51}

In this paper, we report a steady-state isothermal full-cell model for an electrochemical MFC that reduces CO₂ to CO. The model is calibrated and validated using experimental data obtained for a range of feed flow rates and feed compositions. Subsequently, parametric study of several design and operating variables is performed via simulations.

Microfluidic Cell

A MFC (Figure 1a) consists of several parallel and rectangular layers and channels of identical lengths and widths and various heights. These include, from top to bottom, a cathode gas channel, a cathode current collector, a cathode gas diffusion electrode, an aqueous electrolyte channel, an anode gas diffusion electrode, an anode current collector, and an anode gas channel. An aqueous solution enters the electrolyte channel, which is sandwiched between the two gas diffusion electrodes (GDEs). The GDEs are coated with suitable catalysts on the sides of the electrolyte channel to provide a three-phase interface for electrochemical reactions. The current collectors on the other side of the GDEs provide electrical contact between the GDEs and an external potentiostat. The feed gas enters the cathode gas channel and exits the MFC on the other side along with any cathode-side gaseous products. The anode gas channel is either left open to the atmosphere or can be used to collect the anode-side gaseous products. In the latter situation, the inlet is closed, and the anode-side gaseous products exit at the other end.

*Electrochemical Society Active Member.

^zE-mail: chebke@nus.edu.sg; cheiak@nus.edu.sg

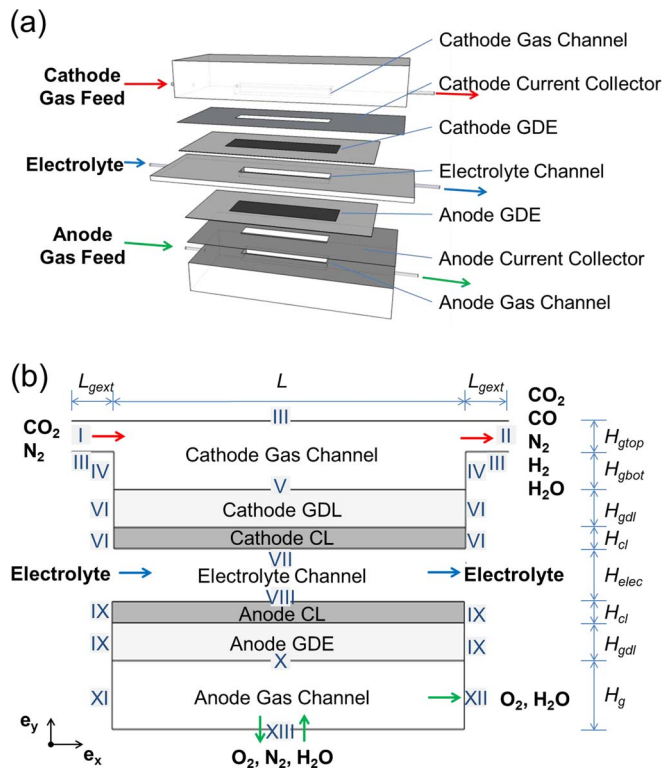
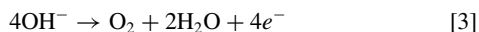


Figure 1. (a) A schematic of the various functional layers in a microfluidic cell for CO_2 reduction and (b) Simplified schematic used in modeling. Boundaries are marked with Roman numerals: (I) cathode gas channel inlet; (II) cathode gas channel outlet; (III) cathode gas channel horizontal walls; (IV) cathode gas channel vertical walls; (V) cathode gas-channel-GDL interface; (VI) cathode GDE vertical walls; (VII) cathode CL-electrolyte interface; (VIII) anode CL-electrolyte interface; (IX) anode GDE vertical walls; (X) anode gas-channel-GDL interface; (XI) anode gas channel wall/inlet; (XII) anode gas channel wall/outlet; (XIII) anode gas channel wall/opening.

For the conversion of CO_2 to CO studied in this work, the feed gas is a mixture of N_2 and CO_2 . The CO_2 in the cathode gas channel diffuses through the top GDE to the cathode catalyst layer (CL). When a neutral or alkaline electrolyte is used, CO_2 is reduced to CO via reaction 1 if a sufficiently high negative cell potential is applied. Water diffuses from the electrolyte to the cathode CL and can be reduced to H_2 via reaction 2. The cathode products CO and H_2 together with H_2O vapor diffuse through the top GDE to the cathode gas channel, and exit the cell with unreacted CO_2 and N_2 .



On the opposite electrode, the oxygen evolution reaction 3 takes place in the anode CL, to balance the OH^- produced and the electrons consumed at the cathode. O_2 and H_2O vapor diffuse through the bottom GDE to the anode gas channel and exit the MFC.



Mathematical Model

The main assumptions underlying our mathematical model are as follows:

- 1) The MFC is at steady-state.
- 2) The system is isothermal. This is a reasonable assumption due to the presence of a flowing liquid (good thermal conductor) electrolyte, and relatively low current density on the order of 10^2 mA/cm^2 in a MFC.

- 3) Variations along the MFC width are negligible, so a 2D model is adequate. In practice, the feed gas can be supplied to the cathode gas channel in several ways such as tube, or rectangular channel. We assume the gas feed inlet to be at the top of the gas channel with a width same as that of the cathode gas channel, but it may have a height less or equal to that of the channel.
- 4) The Ohmic loss across a current collector is negligible. The current collectors can thus be treated as interfaces.
- 5) The rates of the electrochemical reactions can be described by Butler-Volmer kinetic equation, which is commonly invoked in fuel cell models.^{52–56}
- 6) Flow in the gas channel is weakly compressible and laminar. Its Reynolds number is on the order of 10^{-2} .
- 7) The gas diffusion layers (GDLs) and the CLs of the GDEs are homogeneous porous media, so with isotropic porosity and permeability.
- 8) The amount of gaseous species dissolved in the electrolyte is negligible. We assume negligible effective crossover flux of the gaseous species (CO_2 , CO , N_2 , H_2 & O_2) at the electrolyte/CL interface.
- 9) The effective conductivity for ionic transport in the electrolyte phase is constant.

Governing equations.— The simplified schematic of the MFC as modeled in this work is shown in Figure 1b. As shown in the figure, the flow direction is taken to be x-direction and the direction along the height of the cell be y-direction. In the model we take into account the following: multi-component gas transport in the gas channels, porous GDLs and CLs, the material balance in the gas phase (Cathode: CO_2 , N_2 , CO , H_2 and H_2O ; Anode: O_2 , H_2O and N_2), the electronic and ionic charge balance, and charge transfer kinetics. This leads to the following governing equations.

Cathode gas channel.—For a steady 2D flow in the cathode gas channel, the equations for overall mass and momentum balance are:

$$\nabla \cdot (\rho \mathbf{u}) = 0 \quad [4]$$

$$\rho \mathbf{u} \cdot \nabla \mathbf{u} = \rho \mathbf{g} - \nabla p + \nabla \cdot \left[\mu (\nabla \mathbf{u} + (\nabla \mathbf{u})^T) - \frac{2}{3} \mu (\nabla \cdot \mathbf{u}) \mathbf{I} \right] \quad [5]$$

where ρ is the gas density, \mathbf{u} is the velocity vector, \mathbf{g} is the gravitational acceleration, p is the gas pressure, μ is the dynamic gas viscosity, and \mathbf{I} is the identity tensor. For the species mass balance we use

$$\nabla \cdot \mathbf{n}_i = 0 \quad i = \text{CO}_2, \text{CO}, \text{H}_2, \text{H}_2\text{O} \quad [6]$$

where \mathbf{n}_i is the total mass flux of species (the sum of diffusive and convective mass fluxes) i . To calculate multicomponent flux, Maxwell-Stefan equation is used:^{57–60}

$$\mathbf{n}_i = -\rho \omega_i \sum_{j=1}^N D_{ij} \left[\frac{M_g}{M_j} \left(\nabla \omega_j + \omega_j \frac{\nabla M_g}{M_g} \right) + (x_j - \omega_j) \frac{\nabla p}{p} \right] + \rho \omega_i \mathbf{u} \quad i = \text{CO}_2, \text{CO}, \text{H}_2, \text{H}_2\text{O} \quad [7]$$

where ω_i is the mass fraction, x_j is the molar fraction, M_g is the molar mass of the gas mixture:

$$M_g = x_{\text{N}_2} M_{\text{N}_2} + x_{\text{CO}_2} M_{\text{CO}_2} + x_{\text{CO}} M_{\text{CO}} + x_{\text{H}_2} M_{\text{H}_2} + x_{\text{H}_2\text{O}} M_{\text{H}_2\text{O}} \quad [8]$$

and D_{ij} is the multicomponent diffusion coefficient that can be estimated using the empirical correlation recommended by Fuller, Schetler, and Giddings:⁶¹

$$D_{ij} = \frac{1.01325 \times 10^{-2} T^{1.75} \left(\frac{1}{M_i} + \frac{1}{M_j} \right)^{1/2}}{p \left(v_i^{1/3} + v_j^{1/3} \right)} \quad [9]$$

where T is temperature, p is pressure, and v_i is the diffusion volume for molecule i .

The mass fraction of inert N₂ is then computed from the overall mass balance as,

$$\omega_{N_2} = 1 - \omega_{CO_2} - \omega_{CO} - \omega_{H_2} - \omega_{H_2O} \quad [10]$$

Cathode GDL and CL.—For the porous medium (GDL and CL), we use the common equation for the continuity of mass 11 and Brinkman's momentum equation 12:

$$\nabla \cdot (\rho \mathbf{u}) = Q \quad [11]$$

$$\frac{\rho}{\varepsilon} \mathbf{u} \cdot \nabla \frac{\mathbf{u}}{\varepsilon} = \rho \mathbf{g} - \nabla p + \nabla \cdot \left[\frac{\mu}{\varepsilon} \left((\nabla \mathbf{u} + (\nabla \mathbf{u})^T) - \frac{2}{3} (\nabla \cdot \mathbf{u}) \mathbf{I} \right) \right] - \left(\frac{\mu}{\kappa} \right) \mathbf{u} \quad [12]$$

where Q is the mass source term, which occurs only in the CL where the electrochemical reactions taking place, ε is the average porosity and κ is the average permeability of the porous medium. The permeability of the GDL can be predicted using the Tomadakis-Sotirchos model:⁶²

$$\kappa = \frac{\varepsilon}{8 \ln^2 \varepsilon} \frac{(\varepsilon - \varepsilon_p)^{\alpha+2} r_f^2}{(1 - \varepsilon_p)^\alpha [(\alpha + 1)(\varepsilon - \varepsilon_p)]^2} \quad [13]$$

where ε_p is the percolation threshold porosity, the porosity with the least required open void space connectivity for diffusion or permeation through the porous media (here $\varepsilon_p = 0.11$), α is a fitting parameter for through-plan diffusion (here $\alpha = 0.785$), and r_f is the carbon fiber radius (here $r_f = 4.6 \mu m$).⁶³

For species continuity we use:

$$\nabla \cdot \mathbf{n}_i = R_i \quad i = CO_2, CO, H_2, H_2O \quad [14]$$

$$\mathbf{n}_i = -\rho \omega_i \sum_{j=1}^N D_{ij}^{eff} \left[\frac{M_g}{M_j} \left(\nabla \omega_j + \omega_j \frac{\nabla M_g}{M_g} \right) + (x_j - \omega_j) \frac{\nabla p}{p} \right] + \rho \omega_i \quad i = CO_2, CO, H_2, H_2O \quad [15]$$

where R_i is the reaction rate, which accounts for the consumption of reactants and production of products during the electrochemical reactions in the CL, and D_{ij}^{eff} is the effective gas diffusivity in a porous layer, given by the Bruggeman correction⁶⁴ as follows:

$$D_{ij}^{eff} = \varepsilon^{1.5} D_{ij} \quad i = CO_2, CO, H_2, H_2O \quad [16]$$

Again, the mass fraction of N₂ is computed from the overall mass balance, Eq. 10.

Charge conservation at the cathode GDL is imposed by:

$$\nabla \cdot \mathbf{i} = 0 \quad [17]$$

and the current density is given by Ohm's law:

$$\mathbf{i} = -\sigma_{gdl} \nabla \phi_s \quad [18]$$

where σ_{gdl} is the average electronic conductivity of the cathode GDL and ϕ_s is the electric potential of the solid phase of the cathode GDE.

In the CL, current can be split into two parts: ionic current and electronic current. Transport of ions in the liquid phase (electrolyte) forms the ionic current, while transport of electrons in the solid phase (electrode) forms the electronic current. The current conservation equations are obtained using Ohm's law:

$$\nabla \cdot (-\sigma_{cl,s} \nabla \phi_s) = S_s \quad [19]$$

$$\nabla \cdot (-\sigma_{cl,l} \nabla \phi_l) = S_l \quad [20]$$

where $\sigma_{cl,s}$ and $\sigma_{cl,l}$ are the electronic and ionic conductivity of the CL, ϕ_s and ϕ_l are the electric potential of the solid phase and liquid phase in the CL, and S_s and S_l are the current source terms resulting from the electrochemical reactions.

Electrolyte channel.—For the electrolyte channel, the charge conservation 17 holds, and the current follows from Ohm's law as follows:

$$\mathbf{i} = -\sigma_{elec} \nabla \phi_l \quad [21]$$

where σ_{elec} is the average ionic conductivity of the electrolyte and ϕ_l is the electric potential of the liquid electrolyte.

Anode CL and GDL.—If the anode gas channel is open to the atmosphere, convection in the CL and GDL is negligible compared to diffusion. For species continuity we write:

$$\nabla \cdot \mathbf{n}_i = R_i \quad i = O_2, H_2O \quad [22]$$

$$\mathbf{n}_i = -\rho \omega_i \sum_{j=1}^N D_{ij} \left[\frac{M_g}{M_j} \left(\nabla \omega_j + \omega_j \frac{\nabla M_g}{M_g} \right) + (x_j - \omega_j) \frac{\nabla p}{p} \right]$$

$$i = O_2, H_2O \quad [23]$$

Again, the effective diffusivity in the porous layer is modified using the Bruggeman correction. The mass fraction of N₂ is given by

$$\omega_{N_2} = 1 - \omega_{O_2} - \omega_{H_2O} \quad [24]$$

If the O₂ produced at the anode is to be collected, the anode compartment will only have one outlet, so in steady-state only O₂ and H₂O vapor will be present in the anode gas channel and anode GDE. In this case, Eqs. 11–16 can be used to describe the continuity of mass and momentum, and transport of species (O₂ and H₂O) in the porous anode GDL and CL.

The current densities in the anode GDL and CL can be described using Eqs. 17–20.

Anode gas channel.—If the anode gas channel is open to the atmosphere, then we use Eqs. 22–24 for the anode gas channel as well, but with D_{ij} in place of D_{ij}^{eff} . If the compartment is not open to the atmosphere, except for one outlet for the formed O₂ to escape, then we use Eqs. 4–7 for O₂ and H₂O vapor.

Electrochemical reaction kinetics.—In contrast to formate formation in aqueous media, the proposed reaction scheme for CO formation from CO₂ electro-reduction is heterogeneous, involving the adsorption of radicals and further reaction on the metal-catalytic surface.⁴¹ Instead of considering dissolved CO₂, we assume direct adsorption of gaseous CO₂ onto the catalyst surface. For simplicity, we account for only the gas phase species transport in the CL, and use concentration of CO₂ gas instead of dissolved CO₂ in the rate equation.

The rates of the electrochemical reactions are assumed to follow Butler-Volmer kinetics equation, which is commonly invoked in fuel cell models.^{52–56}

Cathode CL.—The rate of formation of CO in the cathode CL depends on the local concentration of CO₂ at the active sites in the CL. As the CL is adjacent to the flowing aqueous electrolyte, it is reasonable to assume the active sites saturated with water and no dependency of water concentration in the rate expression. Thus, the transfer current density corresponding to the formation of CO is given by:

$$i_{CO} = i_{CO,ref} \frac{C_{CO_2}}{C_{CO_2,ref}} \exp \left(-\frac{\alpha_{CO} F}{RT} \eta_{CO} \right) \quad [25]$$

where $i_{CO,ref}$ is the exchange current density, C_{CO_2} is the local CO₂ concentration, $C_{CO_2,ref}$ is the reference CO₂ concentration, α_{CO} is the charge transfer coefficient, F is the Faraday constant, R is the universal gas constant, T is the system temperature, and η_{CO} is the overpotential of the CO formation reaction at the cathode. The CO overpotential is given by:

$$\eta_{CO} = \phi_s - \phi_l - E_{CO} \quad [26]$$

where E_{CO} is the reversible potential of the half reaction for CO formation, ϕ_s and ϕ_l are the local electric and electrolyte potential derived from Eq. 19 and Eq. 20.

The experiments by Whipple⁶⁵ revealed that cell performance is independent of electrolyte pH for the electrochemical reduction of

CO₂ to CO in a microfluidic cell using an aqueous flowing electrolyte. Thus, the kinetics of water electrolysis can be treated as independent of the concentrations of H⁺ and OH⁻ ions under the range of operating conditions studied. The transfer current density corresponding to the formation of H₂ at the cathode then can be expressed as:

$$i_{\text{H}_2} = i_{\text{H}_2,\text{ref}} \exp\left(-\frac{\alpha_{\text{H}_2} F}{RT} \eta_{\text{H}_2}\right) \quad [27]$$

where $i_{\text{H}_2,\text{ref}}$ is the exchange current density and α_{H_2} is the charge transfer coefficient for this reaction. The overpotential η_{H_2} is given by:

$$\eta_{\text{H}_2} = \phi_s - \phi_l - E_{\text{H}_2} \quad [28]$$

where E_{H_2} is the reversible potential of the half reaction for H₂ formation.

The reaction rates R_i at the cathode CL in Eq. 14 are then given by:

$$\begin{aligned} R_{\text{CO}_2} &= -\frac{a_{\text{CO}} i_{\text{CO}}}{2F} M_{\text{CO}_2}, & R_{\text{H}_2\text{O}} &= -\frac{a_{\text{CO}} i_{\text{CO}}}{2F} M_{\text{H}_2\text{O}} - \frac{a_{\text{H}_2} i_{\text{H}_2}}{F} M_{\text{H}_2\text{O}} \\ R_{\text{CO}} &= \frac{a_{\text{CO}} i_{\text{CO}}}{2F} M_{\text{CO}}, & R_{\text{H}_2} &= \frac{a_{\text{H}_2} i_{\text{H}_2}}{2F} M_{\text{H}_2} \end{aligned} \quad [29]$$

where a_{CO} and a_{H_2} are the specific surface (ratio of reaction surface of the active sites to catalyst layer volume).

The mass source term Q in Eq. 11 is then given by:

$$Q = R_{\text{CO}_2} + R_{\text{CO}} + R_{\text{H}_2} + R_{\text{H}_2\text{O}} \quad [30]$$

The current source terms S_s and S_l in Eq. 19 and Eq. 20 are given by:

$$S_s = -(a_{\text{CO}} i_{\text{CO}} + a_{\text{H}_2} i_{\text{H}_2}), \quad S_l = a_{\text{CO}} i_{\text{CO}} + a_{\text{H}_2} i_{\text{H}_2} \quad [31]$$

Anode CL.—At the anode CL, only O₂ formation reaction takes place. The transfer current density for O₂ formation reaction can be described by:

$$i_{\text{O}_2} = i_{\text{O}_2,\text{ref}} \exp\left(\frac{\alpha_{\text{O}_2} F}{RT} \eta_{\text{O}_2}\right) \quad [32]$$

where $i_{\text{O}_2,\text{ref}}$ is the exchange current density and α_{O_2} the charge transfer coefficient for this reaction. The overpotential η_{O_2} is given by:

$$\eta_{\text{O}_2} = \phi_s - \phi_l - E_{\text{O}_2} \quad [33]$$

where E_{O_2} is the reversible potential of the half reaction for O₂ formation.

The reaction rates R_i at the anode CL in Eq. 22 are then given by:

$$R_{\text{O}_2} = \frac{a_{\text{O}_2} i_{\text{O}_2}}{4F} M_{\text{O}_2}, \quad R_{\text{H}_2\text{O}} = \frac{a_{\text{O}_2} i_{\text{O}_2}}{2F} M_{\text{H}_2\text{O}} \quad [34]$$

The mass source term Q in Eq. 11 is then given by:

$$Q = R_{\text{O}_2} + R_{\text{H}_2\text{O}} \quad [35]$$

The current source terms S_s and S_l in Eqs. 19 and 20 are given by:

$$S_s = a_{\text{O}_2} i_{\text{O}_2}, \quad S_l = -a_{\text{O}_2} i_{\text{O}_2} \quad [36]$$

The overall applied cell potential is defined as:

$$V_{\text{cell}} = V_{\text{cath}} - V_{\text{anod}} \quad [37]$$

where V_{cath} and V_{anod} are the electric potentials applied at the cathode and anode current collectors respectively.

Boundary conditions.—*Cathode gas channel.*—At the cathode gas inlet (I), composition and flow rate are constant:

$$\mathbf{u} \cdot \mathbf{e}_x = U_{g,\text{in}}, \quad \omega_{\text{CO}_2} = \omega_{\text{CO}_2,\text{in}}, \quad \omega_{\text{CO}} = 0, \quad \omega_{\text{H}_2} = 0, \quad \omega_{\text{H}_2\text{O}} = 0 \quad [38]$$

where \mathbf{e}_x is the unit vector in the x-direction, i.e. along the flow direction, $U_{g,\text{in}}$ is the average normal inflow velocity, and $\omega_{\text{CO}_2,\text{in}}$ is the mass fraction of CO₂ in the feed gas.

At the cathode gas outlet boundary (II), we assume a constant reference pressure p_{exit} and fully developed flow with no viscous stress and no diffusive species fluxes:

$$\begin{aligned} p &= p_{\text{exit}}, \quad \left(\mu (\nabla \mathbf{u} + (\nabla \mathbf{u})^T) - \frac{2}{3} \mu (\nabla \cdot \mathbf{u}) \mathbf{I} \right) \mathbf{e}_x = 0 \\ \mathbf{n}_i \cdot \mathbf{e}_x &= 0 \quad i = \text{CO}_2, \text{CO}, \text{H}_2, \text{H}_2\text{O} \end{aligned} \quad [39]$$

At the outer walls of the cathode gas channel (III & IV), we assume that the no-slip condition applies and that the walls are impermeable:

$$\mathbf{u} \cdot \mathbf{e}_y|_{\text{III}} = 0, \quad \mathbf{n}_i \cdot \mathbf{e}_y|_{\text{III}} = 0 \quad i = \text{CO}_2, \text{CO}, \text{H}_2, \text{H}_2\text{O} \quad [40]$$

$$\mathbf{u} \cdot \mathbf{e}_x|_{\text{IV}} = 0, \quad \mathbf{n}_i \cdot \mathbf{e}_x|_{\text{IV}} = 0 \quad i = \text{CO}_2, \text{CO}, \text{H}_2, \text{H}_2\text{O} \quad [41]$$

Cathode gas-channel-GDL interface.—The electric potential at this interface is the applied cathode potential V_{cath} :

$$\phi_s = V_{\text{cath}} \quad [42]$$

Cathode GDL and CL.—At the vertical walls of the porous GDL and CL (VI), we specify no normal flow, no species fluxes (impermeable walls), and charge insulation,

$$\mathbf{u} \cdot \mathbf{e}_x = 0, \quad \mathbf{n}_i \cdot \mathbf{e}_x = 0, \quad \mathbf{i} \cdot \mathbf{e}_x = 0 \quad i = \text{CO}_2, \text{CO}, \text{H}_2, \text{H}_2\text{O} \quad [43]$$

Cathode CL-electrolyte interface.—We assume no normal flow and no crossover fluxes at this interface (VII):

$$\mathbf{u} \cdot \mathbf{e}_y = 0, \quad \mathbf{n}_i \cdot \mathbf{e}_y = 0 \quad i = \text{CO}_2, \text{CO}, \text{H}_2, \text{H}_2\text{O} \quad [44]$$

Water in the electrolyte is in equilibrium with H₂O vapor in the gas phase. The mass fraction of H₂O vapor at this interface can be calculated from its vapor pressure p_{sat} :

$$\omega_{\text{H}_2\text{O}} = \frac{p_{\text{sat}} M_{\text{H}_2\text{O}}}{p M_g} \quad [45]$$

where M_g is the molar mass of the gas mixture.

Anode CL-electrolyte interface.—We assume normal flow, no crossover fluxes and saturated H₂O vapor at this interface (VIII):

$$\mathbf{u} \cdot \mathbf{e}_y = 0, \quad \mathbf{n}_{\text{O}_2} \cdot \mathbf{e}_y = 0, \quad \omega_{\text{H}_2\text{O}} = \frac{p_{\text{sat}} M_{\text{H}_2\text{O}}}{p M_g} \quad [46]$$

Anode GDL and CL.—At the vertical walls of the porous GDL and CL (IX), we specify no normal flow, no species fluxes (impermeable walls), and charge insulation,

$$\mathbf{u} \cdot \mathbf{e}_x = 0, \quad \mathbf{n}_i \cdot \mathbf{e}_x = 0, \quad \mathbf{i} \cdot \mathbf{e}_x = 0 \quad i = \text{O}_2, \text{H}_2\text{O} \quad [47]$$

Anode gas-channel-GDL interface.—The electric potential at this interface equals the applied anode potential V_{anod} :

$$\phi_s = V_{\text{anod}} \quad [48]$$

Anode gas channel.—If the anode is open to the atmosphere, then both inlet and outlet of the gas channel are closed and the wall (XIII) is open. At the vertical walls (XI and XII), we specify no diffusive fluxes:

$$\mathbf{n}_i \cdot \mathbf{e}_x|_{\text{XI}} = 0, \quad \mathbf{n}_i \cdot \mathbf{e}_x|_{\text{XII}} = 0 \quad [49]$$

and at the opening (XIII), we specify a constant mass fraction of O₂ as it is exposed to the atmosphere which can be considered as a bulk phase of constant composition:

$$\omega_{\text{O}_2} = \omega_{\text{O}_2,\text{ref}} \quad [50]$$

If the O₂ produced is to be collected, then the inlet (XI) is still closed, but the outlet (XII) is open. We apply no-slip condition to the inlet (XI) and the horizontal wall (XIII):

$$\mathbf{u} \cdot \mathbf{e}_x|_{\text{XI}} = 0, \quad \mathbf{u} \cdot \mathbf{e}_y|_{\text{XIII}} = 0 \quad [51]$$

Table I. Key parameter values used in simulation.

Parameter	Symbol	Base Case / (Range)	Unit	Source
<i>Operating Condition</i>				
Temperature	T	298	K	measured
Exit Pressure	P_{exit}	1.0	atm (abs)	measured
Feed gas flow rate	Q_g	7 / (2–42)	sccm	measured
Feed CO ₂ molar fraction	$x_{CO_2, in}$	0.2 / (0.05–0.35)	-	measured
Applied cell potential	V_{cell}	-3.0 / (-2.2–-3.2)	V	measured
pH	pH	7.0	-	measured
<i>MFC Geometry</i>				
Channel length	L	0.02 / (0.01–0.4)	m	measured
Extended length of the gas channel	L_{gext}	0.002	m	measured
Width of the channel	W	0.005	m	measured
Height of the upper portion of the gas channel	H_{gtop}	5.08×10^{-4}	m	measured
Height of the lower portion of the gas channel	H_{gbot}	1.49×10^{-3}	m	measured
Height of the GDL	H_{gdl}	3.00×10^{-4}	m	measured
Height of the CL	H_{cl}	8×10^{-6}	m	63
Height of the electrolyte channel	H_{elec}	1.50×10^{-3}	m	measured
<i>Fluidic Properties</i>				
Dynamic viscosity of gas (estimated using N ₂)	μ	1.7855×10^{-5}	Pa · s	68
Ionic conductivity of the electrolyte	σ_{elec}	15.0	S/m	calculated for 1M of KCl ⁶⁹
Water vapor pressure	p_{sat}	3187.7	Pa (abs)	70
Diffusion volume for CO ₂	v_{CO_2}	26.9	-	61,68
Diffusion volume for CO	v_{CO}	18.9	-	61,68
Diffusion volume for H ₂	v_{H_2}	6.12	-	61,68
Diffusion volume for N ₂	v_{N_2}	17.9	-	61,68
Diffusion volume for O ₂	v_{O_2}	16.6	-	61,68
Diffusion volume for H ₂ O	v_{H_2O}	12.7	-	61,68
<i>Electrode Properties</i>				
Porosity of GDL	ϵ	0.663/(0.4–0.8)	-	63
Porosity of CL	ϵ_{cl}	0.4	-	54
Electronic conductivity of the GDL	σ_s	50000	S/m	63
Electronic conductivity of the solid phase of CL	$\sigma_{cl,s}$	0.727×10^5	S/m	54
Ionic conductivity of the liquid phase of CL	$\sigma_{cl,l}$	0.0657	S/m	54

At the outlet, we specify a reference pressure and assume no viscous stress,

$$p = p_{exit}, \left(\mu (\nabla \mathbf{u} + (\nabla \mathbf{u})^T) - \frac{2}{3} \mu (\nabla \cdot \mathbf{u}) \mathbf{I} \right) \mathbf{e}_x = 0 \quad [52]$$

Cell performance.— Current Densities.— Current density reflects the rate of an electrochemical reaction. The computed average partial current density is the integrated average of the local current densities at the cathode CL for a given species:

$$i_{CO}^{num} = \frac{1}{L} \int_0^{H_{cl}} \int_0^L a_{CO} i_{CO} dx dy \quad [53]$$

$$i_{H_2}^{num} = \frac{1}{L} \int_0^{H_{cl}} \int_0^L a_{H_2} i_{H_2} dx dy \quad [54]$$

Specifically, the average partial current density i_{CO}^{num} reflects CO₂ conversion rate.

Then, the computed average total current density is:

$$i_{total}^{num} = i_{CO}^{num} + i_{H_2}^{num} \quad [55]$$

Faradaic efficiency.—This reflects the selectivity of the primary reaction (here CO formation). It is computed using the following equation:

$$FE(\%) = \frac{i_{CO}^{num}}{i_{total}^{num}} \times 100\% \quad [56]$$

Conversion per pass.—The conversion of CO₂ per pass is specified by:

$$\text{Conv}(\%) = \frac{\int_0^{H_{gtop}} \mathbf{n}_{CO_2} \cdot \mathbf{e}_x |_{II} dy - \int_0^{H_{gtop}} \mathbf{n}_{CO_2} \cdot \mathbf{e}_x |_{I} dy}{\int_0^{H_{gtop}} \mathbf{n}_{CO_2} \cdot \mathbf{e}_x |_{I} dy} \times 100\% \quad [57]$$

Numerical method.— We implemented Eqs. 4–57 in COMSOL 4.3b using the base case parameters in Table I, and solved them using the finite element method. We began with a coarse mesh of about 2500 elements for the unit cell in Figure 2. Consecutive mesh adaptation of up to 120000 elements allowed for high resolution in the GDEs. Mesh independence was ensured by ensuring that successive mesh adaptations did not change CO₂ conversion by more than 0.1%. One simulation takes 3–8 minutes on an Intel Core i7–3770 CPU @ 3.40 GHz PC with 16.0 GB RAM.

Experimental

The kinetic parameters in Eq. 25, 27 and 32 are system specific and must be fitted with the help of experimental data. Our reactor design and experimental setup were similar to the experimental study by Whipple et al.¹³ The electrolyte channel was prepared by machining a 0.5 cm wide by 2.0 cm long channel in a 1.5 mm thick polyether ether ketone (PEEK) window. The GDEs were prepared by applying catalyst ink via hand-painting on Sigracet 35BC gas diffusion layers (GDLs, Ion Power). Catalyst loading was 0.9 mg Ag/cm² and 1.0 mg Pt/cm² for the cathode and anode respectively. The cathode gas channel was a 0.5 cm wide by 2.0 cm long by 2 mm deep window in an aluminum block. The anode was left open to the atmosphere. The assembly was held together with 4 bolts with Teflon washers to

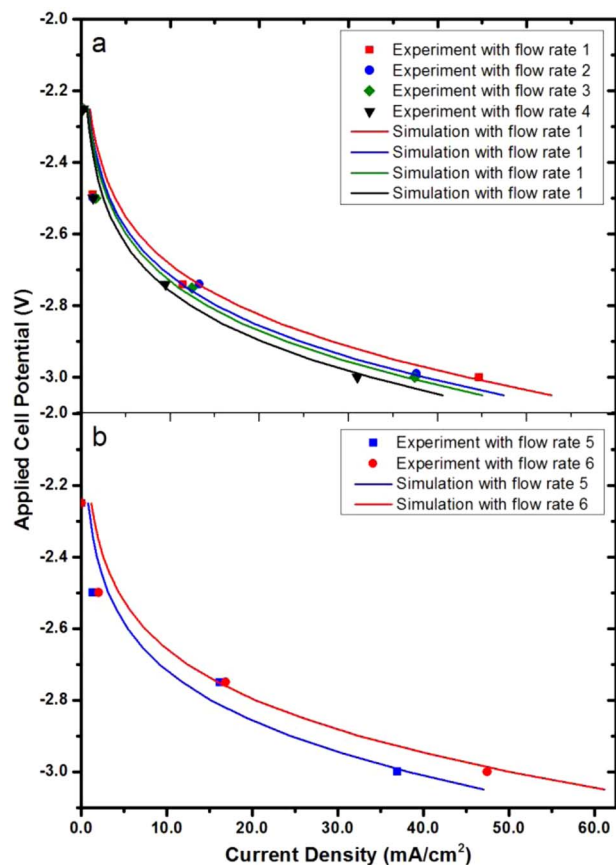


Figure 2. Comparison of polarization curves for (a) parameter fitting and (b) model validation. Feed gas flow rate and compositions are specified in Table II. Other operating conditions take the base case values in Table I.

maintain electric isolation between electrodes. The dimensions and material properties of the MFC are summarized in Table I as base case values.

The experiments were conducted at room temperature (298 K) with the outlet streams exposed to ambient pressure (1.0 atm). An aqueous stream of 1 M KCl at a flow rate of 0.4 ml/min was used as the electrolyte. The experiments were performed at six feed gas flows as summarized in Table II. For each flow, the cell potential was varied from -2.25 V to -3.00 V at -0.25 V intervals. Thus, 24 independent data sets were obtained. Cell polarization curves were recorded by steady-state chrono-amperometric measurements. Individual anode and cathode polarization curves were measured using a Ag/AgCl reference electrode (RE-5B, BASi) that was placed in the outlet reservoir of the electrolyte.

Parameter Fitting and Model Verification

To obtain the best fits for the six kinetic parameters (α_{CO} , α_{H_2} , α_{O_2} , $a_{CO}i_{CO,ref}$, $a_{H_2}i_{H_2,ref}$ and $a_{O_2}i_{O_2,ref}$), the discrepancy between simulated and experimental results needs to be minimized. To this end, we define mean sum of squared errors (MSE) between

Experimental No.	Parameter Fitting				Validation	
	1	2	3	4	5	6
Feed CO ₂ flow rate (sccm)	1.5	1.5	1.5	1.5	1.4	3.0
Feed N ₂ flow rate (sccm)	4.6	6.1	7	9	5.6	7.0

experimental and simulated (numerical) average current densities as the objective function:

$$MSE = \sqrt{\frac{1}{16} \sum_{k=1}^{16} (i_{total}^{num} - i_{total}^{exp})^2} \quad [58]$$

where k is the index for the 16 experimental runs used for parameter fitting.

Another measure for the quality of the fit is the percent error in the individual current density, which quantifies the error associated with each simulated average current density when the experimental data is available and is non-zero:

$$err_i (\%) = \frac{i_i^{num} - i_i^{exp}}{i_i^{exp}} \times 100\% \quad [59]$$

We exported our COMSOL model into MATLAB 2012b and used a coordinate search global optimization algorithm (DIRECT)^{66,67} to minimize the function in Eq. 57. The best-fit parameters are shown in Table III. Figure 2 compares the experimentally measured polarization curves with the model predictions. Good agreement is observed with $MSE = 1.34$ (mA/cm²) during fitting the electrochemical reaction kinetic parameters and $MSE = 2.22$ (mA/cm²) during model validation. The fit at the high cell potentials of around -3.0 V is very good, with an average percent error of 3.3% during fitting and 4.5% during validation. This is desirable, as the cell will usually operate at potentials negative than -2.5 V.

Results and Discussion

Electrochemical characteristics.— Figure 3 presents the simulated current-potential profiles. As the applied cell potential increases (becomes more negative), the current densities for both CO and H₂ formations increase. The undesirable side reaction of H₂ formation accounts for less than 10% of the total current density for applied cell potentials below -2.8 V. A more negative cell potential is required for the onset of H₂ formation compared to CO formation. This is expected because the exchange current density corresponding to H₂ formation is 3 order of magnitude smaller than that for CO formation. As predicted by the larger charge transfer coefficient, H₂ production increases much faster than CO formation at high cell potentials, leading to a decrease in the faradaic efficiency. Thus, if CO is the only desired product, an intermediate optimal potential exists. In contrast, for syngas production, a suitable potential should be chosen to obtain the desired CO to H₂ ratio.

Effects of feed CO₂ concentration.— Figure 4 shows the effects of CO₂ concentration on cell performance for fixed feed gas flow rates.

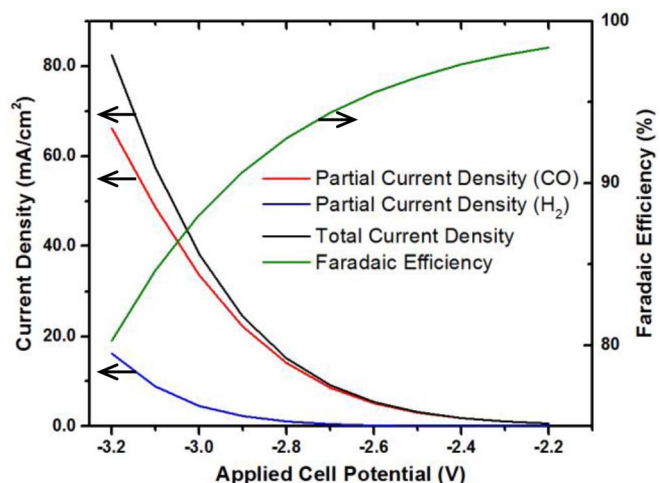
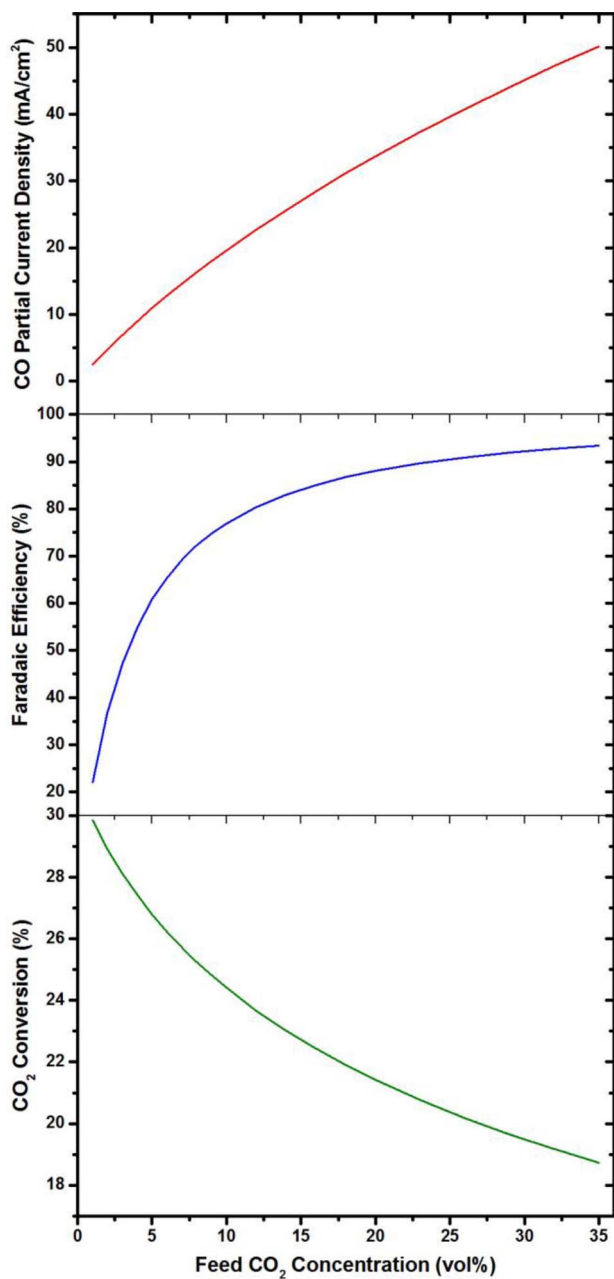
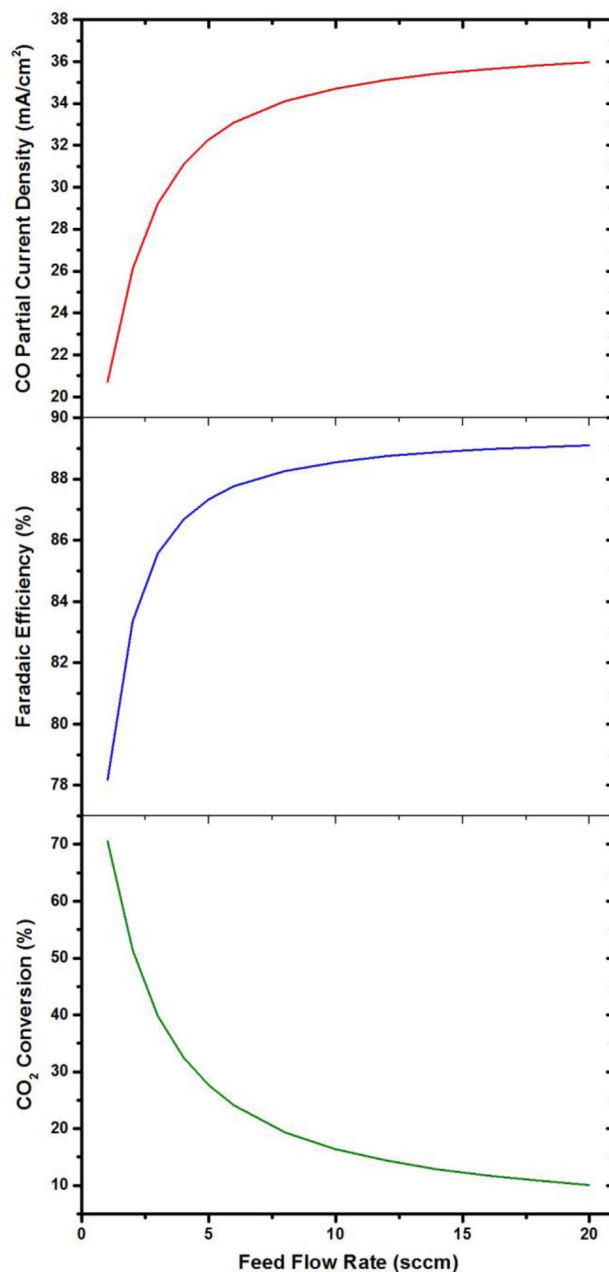


Figure 3. Effects of applied cell potential on cell performance. Operating conditions except for cell potential take the base case value in Table I.

Table III. Parameters in the electrochemical reaction kinetic equations.

Parameter	Symbol	Value	Unit
Reversible potential of CO formation half-cell	E_{CO}	-0.52	V (at pH 7 vs SHE)
Reversible potential of H ₂ formation half-cell	E_{H_2}	0.41	V (at pH 7 vs SHE)
Reversible potential of O ₂ formation half-cell	E_{O_2}	0.82	V (at pH 7 vs SHE)
Reference CO ₂ concentration	$C_{CO_2,ref}$	40.9	mol/m ³
Exchange current density × specific surface, CO formation	$a_{CO}i_{CO,ref}$	1.28×10^5	A/m ³
Exchange current density × specific surface, H ₂ formation	$a_{H_2}i_{H_2,ref}$	48.3	A/m ³
Exchange current density × specific surface, O ₂ formation	$a_{O_2}i_{O_2,ref}$	9.98×10^{-2}	A/m ³
Charge transfer coefficient of CO formation half-cell	α_{CO}	0.17	-
Charge transfer coefficient of H ₂ formation half-cell	α_{H_2}	0.25	-
Charge transfer coefficient of O ₂ formation half-cell	α_{O_2}	0.79	-

**Figure 4.** Effects of feed CO₂ concentration on cell performance. Operating conditions except feed CO₂ concentration take the base case values in Table I.**Figure 5.** Effects of the volumetric flow rate of the gas feed on cell performance. Operating conditions except for feed gas flow rate take the base case values in Table I.

The average partial current density for CO formation demonstrates a nearly linear increase from 2.5 mA/cm² to 50 mA/cm² as CO₂ concentration of the feed increases from 1 vol% to 35 vol%. The faradaic efficiency increases from 22% to 77%, while the CO₂ conversion decreases from 30% to 24%, for an initial increase from 1 vol% to 10 vol% in the CO₂ concentration of the feed. However, upon a further increase in CO₂ concentration, the rate of increase in faradaic efficiency and the rate of decrease in CO₂ conversion drop. As the CO₂ concentration in the feed increases, its concentration at the active sites in the CL also increases, leading to an increase in current density and faradaic efficiency. This confirms that the kinetics for CO₂ reduction depends significantly on the CO₂ concentration at the active sites. Therefore, modifying the GDEs such that they enhance CO₂ transport to the CL is critical for improving cell performance.

Effects of feed gas flow rate.— The effects of the feed gas flow rate at constant CO₂ concentrations on cell performance are shown in Figure 5. As the feed gas flow rate increases from 1 to 6 sccm, the average CO partial current density increases by more than 50% and the faradaic efficiency increases from 78% to 88%. At higher feed rate, the average CO₂ concentration in the flow channel is higher and thus a higher CO₂ concentration is present in the CL. Therefore, higher feed gas flow increases the rate of reaction and thus current density. However, when the CO₂ concentration in the CL exceeds a certain limit, the effect of overpotential dominates over mass transport. Any further increase in that concentration has a negligible effect on the reaction kinetics. This is confirmed by the fact that the CO partial current density and faradaic efficiency level off when the feed rate exceeds 15 sccm. A higher feed rate also implies a shorter residence time. The decrease in residence time cannot be compensated by the increase in reaction kinetics, resulting in a decrease in CO₂ conversion,

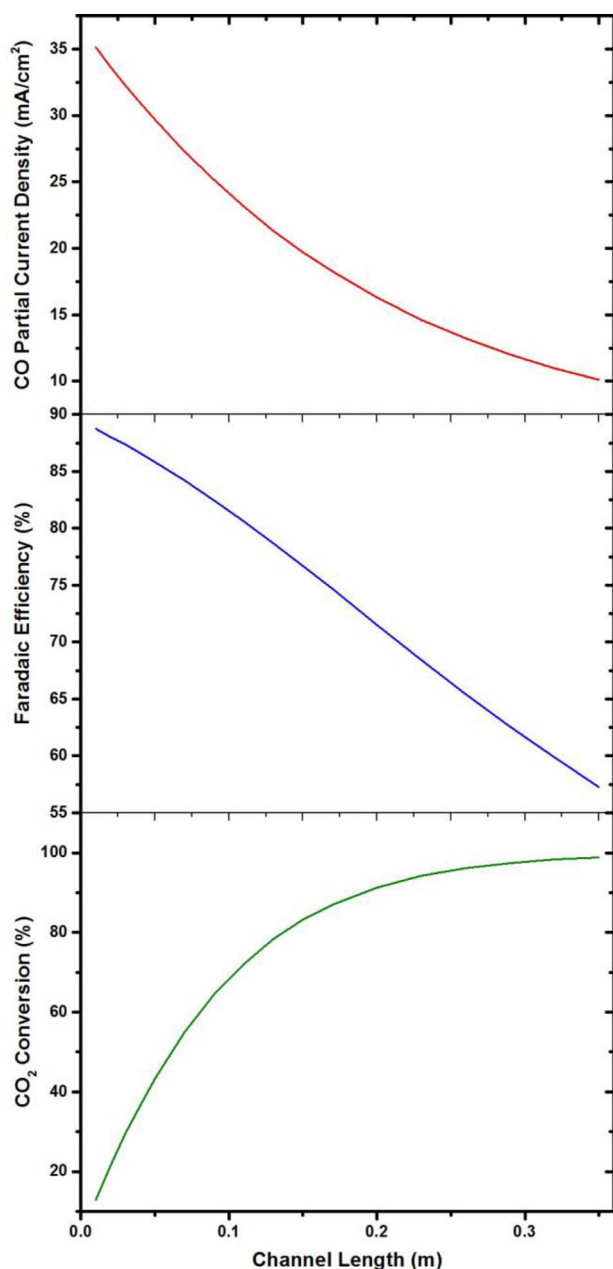


Figure 6. Effects of channel length on cell performance. Operating conditions and cell dimensions except for channel length take the base case values in Table I.

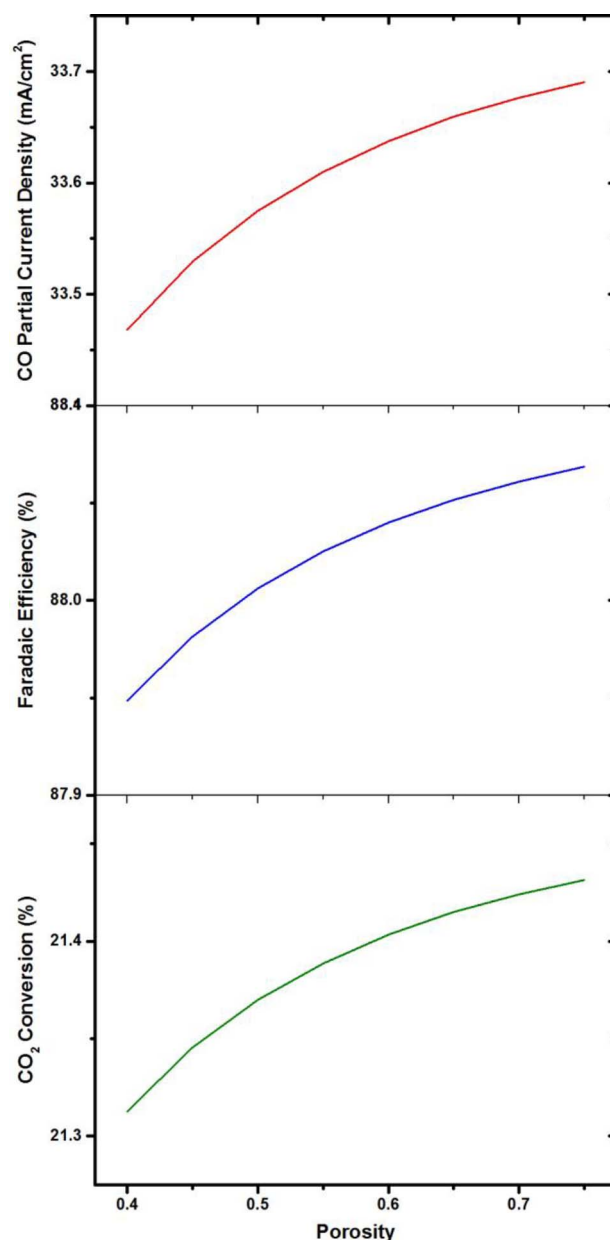


Figure 7. Effects of GDE porosity on cell performance. Operating conditions take the base case values in Table I.

as shown in Figure 5. Operating the reactor at higher feed rate and thus higher throughput is desirable, as it lowers both the operating cost (high faradaic efficiency) and capital cost (higher CO₂ conversion rate (mol/m²-s)).

Effects of channel length.— From a design perspective, analyzing the effect of channel length on cell performance is useful. As demonstrated in Figure 6, upon increasing the channel length from 0.01 m to 0.35 m, the CO₂ conversion increases from 13% to 99%, but the average partial current density corresponding to CO formation drops from 35 mA/cm² to 10 mA/cm² and the faradaic efficiency decreases almost linearly from 89% to 57%. The former can be explained by the fact that a longer channel leads to a larger active surface for electrochemical reaction, thus improving CO₂ conversion. However, longer channel leads to lower average CO₂ concentration in the cell because of depletion of the reactant CO₂ and dilution effect of the product gaseous CO and H₂, resulting in smaller average current density. The side reaction (H₂ evolution) is independent of the composition of the gas in the channel, so the electrical energy consumption associated with the side reaction increases with channel length, resulting in a decrease in the faradaic efficiency. During design, we can use this model to determine the minimum channel length for a given CO₂ conversion.

Effects of electrode porosity.— The effect of increasing the porosity of GDL on cell performance is shown in Figure 7. Increased porosity indeed leads to a higher faradaic efficiency, CO₂ conversion and CO partial current density. However, the improvements are less than 1% for all the three performance measures for a porosity change from 0.40 to 0.75. This suggests that considering porosity of the GDL is not needed in optimizing cells for better performance.

Conclusions

We have presented a 2D isothermal electrochemical model for CO₂ reduction to CO in a microfluidic flow cell. The model accounts for all significant physics and electrochemistry in the cell such as the transport of species and charges, momentum and mass conservation, and electrochemical reactions. Simulation results successfully predict a set of polarization curves obtained at different feed gas flow rate and gas feed compositions. The prediction is better at high cell potentials (−2.5 to −3 V), where the cell usually operates, with an average percent error of 3.4%. Simulation results also reveal the importance of improving CO₂ transport in the GDEs, as well as the limited effects on cell performance of the CO₂ concentration in the feed, the flow rate of the gaseous feed, the channel length, and the GDE porosity. Further analysis with the multiphysics model can guide further design and optimization of the promising MFC architecture for CO₂ reduction to CO. Moreover, this model can be extended from a single cell to cell stack, and subsequently used for the design and optimization of large systems.

List of Symbols

a_i	specific surface (ratio of reaction surface of the active sites to catalyst layer volume), 1/m
C_i	concentration of species i , mol/m ³
Conv	Conversion of CO ₂ per pass
D_{ij}	multicomponent diffusion coefficients, m ² /s
\mathbf{e}	unit normal vector
err	error
E_i	reversible potential of the half-cell corresponding to formation of species i , V
F	Faradaic constant, 96485 C/mol
\mathbf{g}	acceleration due to gravity, m/s ²
H	height, m
\mathbf{i}	current density, A/m ²
i_i	transfer current density corresponding to the formation of species i , A/m ²

$i_{i,\text{ref}}$	exchange current density corresponding to the formation of species i , A/m ²
\mathbf{I}	identity tensor
L	channel length, m
M_i	molecular mass of species i , kg/mol
\mathbf{n}_i	mass flux of species i , kg/(m ² · s)
N	number of species
p	pressure of gas, Pa
Q	mass source term, kg/(m ³ · s)
r_f	carbon fiber radius in the diffusion layer, m
R	universal gas constant, 8.314 J/mol · K
R_i	reaction rate of species i in the electrochemical reaction, kg/(m ³ · s)
S	current source term, A/m ³
T	temperature, K
\mathbf{u}	velocity, m/s
$U_{g,\text{in}}$	Average normal inflow velocity, m/s
v_i	diffusion volume of molecule i , used in the correlation by Fuller, Schettler, and Giddings
V	applied potential, V
V_i	molar volume of species i , m ³ /mol
W	width, m
x_i	molar fraction of species i

Greek

α	fitting parameter for through-plane diffusion in the Tomadakis-Sotirchos model
α_i	charge transfer coefficient of the half-cell corresponding to the formation of species i
ε	porosity of the gas diffusion layer or catalyst layer
ε_p	percolation threshold porosity, used in the Tomadakis-Sotirchos model
η_i	overpotential of the formation reaction species i , V
κ	permeability of the gas diffusion layer or catalyst layer, m ²
μ	dynamic viscosity, kg/m · s
ρ	density of gas, kg/m ³
σ	electric conductivity, S/m
ϕ	electric potential
ω_i	mass fraction of species i

Subscripts

anod	at the anode
cath	at the cathode
cell	for the whole cell
cl	catalyst layer
cl_l	liquid phase in the catalyst layer
cl_s	solid phase in the catalyst layer
elec	at the electrolyte
exit	At the exit
f	carbon fiber
gbot	lower portion of the gas channel
gdl	gas diffusion layer
gext	extended length of the gas channel
gtop	upper portion of the gas channel
i	species
in	at the inlet or in the feed
j	species
k	experiment number
l	liquid phase
p	percolation threshold
ref	reference
s	solid phase
sat	saturated
total	total
x	along the flow direction
y	along the height of the cell direction

Superscripts

eff	effective
exp	experimental
num	numerical
T	transpose

References

- C. Le Quéré, G. P. Peters, R. J. Andres, R. M. Andrew, T. Boden, P. Ciais, P. Friedlingstein, R. A. Houghton, G. Marland, R. Moriarty, S. Sitch, P. Tans, A. Armeth, A. Arvanitis, D. C. E. Bakker, L. Bopp, J. G. Canadell, L. P. Chini, S. C. Doney, A. Harper, I. Harris, J. I. House, A. K. Jain, S. D. Jones, E. Kato, R. F. Keeling, K. Klein Goldewijk, A. Körtzinger, C. Koven, N. Lefèvre, A. Omar, T. Ono, G. H. Park, B. Pfeil, B. Poulter, M. R. Raupach, P. Regnier, C. Rödenbeck, S. Saito, J. Schwinger, J. Segsneider, B. D. Stocker, B. Tilbrook, S. van Heuven, N. Viovy, R. Wanninkhof, A. Wiltshire, S. Zaehle, and C. Yue, *Earth Syst. Sci. Data Discuss.*, **6**, 689 (2013).
- K. S. Lackner, *Annual Review of Energy and the Environment*, **27**, 193 (2002).
- G. Centi and S. Perathoner, *Catalysis Today*, **148**, 191 (2009).
- S. I. Plasynski, J. T. Litynski, H. G. McIlvried, and R. D. Srivastava, *Critical Reviews in Plant Sciences*, **28**, 123 (2009).
- Gateway to the UN System's Work on Climate Change, <http://www.un.org/wcm/content/site/climatechange/pages/gateway/mitigation>.
- W. M. Budzianowski, *Energy*, **41**, 280 (2012).
- D. T. Whipple and P. J. A. Kenis, *The Journal of Physical Chemistry Letters*, **1**, 3451 (2010).
- T. Yamamoto, D. A. Tryk, A. Fujishima, and H. Ohta, *Electrochimica Acta*, **47**, 3327 (2002).
- S. H. Jensen, X. Sun, S. D. Ebbesen, R. Knibbe, and M. Mogensen, *International Journal of Hydrogen Energy*, **35**, 9544 (2010).
- C. Delacourt, P. L. Ridgway, J. B. Kerr, and J. Newman, *Journal of The Electrochemical Society*, **155**, B42 (2008).
- F. Bidrawn, G. Kim, G. Corre, J. T. S. Irvine, J. M. Vohs, and R. J. Gorte, *Electrochemical and Solid-State Letters*, **11**, B167 (2008).
- S. Uhm and Y. D. Kim, *Current Applied Physics*, **14**, 672 (2014).
- D. T. Whipple, E. C. Finke, and P. J. A. Kenis, *Electrochemical and Solid-State Letters*, **13**, B109 (2010).
- B. A. Rosen, A. Salehi-Khojin, M. R. Thorson, W. Zhu, D. T. Whipple, P. J. Kenis, and R. I. Masel, *Science*, **334**, 643 (2011).
- M. R. Thorson, K. I. Siil, and P. J. A. Kenis, *Journal of the Electrochemical Society*, **160**, F69 (2012).
- Y. Hori, H. Wakebe, T. Tsukamoto, and O. Koga, *Electrochimica Acta*, **39**, 1833 (1994).
- G. B. Stevens, T. Reda, and B. Raguse, *Journal of Electroanalytical Chemistry*, **526**, 125 (2002).
- J. Shi, F. Shi, N. Song, J.-X. Liu, X.-K. Yang, Y.-J. Jia, Z.-W. Xiao, and P. Du, *Journal of Power Sources*, 2014.
- S. Kaneco, R. Iwao, K. Iiba, K. Ohta, and T. Mizuno, *Energy*, **23**, 1107 (1998).
- M. N. Mahmood, D. Masheder, and C. J. Hartly, *Journal of Applied Electrochemistry*, **17**, 1159 (1987).
- N. Furuya, T. Yamazaki, and M. Shibata, *Journal of Electroanalytical Chemistry*, **431**, 39 (1997).
- R. L. Cook, R. C. MacDuff, and A. F. Sammells, *Journal of The Electrochemical Society*, **137**, 607 (1990).
- S. Kaneco, H. Katsumata, T. Suzuki, and K. Ohta, *Energy & Fuels*, **20**, 409 (2005).
- S. Kaneco, N.-h. Hiei, Y. Xing, H. Katsumata, H. Ohnishi, T. Suzuki, and K. Ohta, *Electrochimica Acta*, **48**, 51 (2002).
- S. Kaneco, K. Iiba, N.-h. Hiei, K. Ohta, T. Mizuno, and T. Suzuki, *Electrochimica Acta*, **44**, 4701 (1999).
- S. Kaneco, H. Katsumata, T. Suzuki, and K. Ohta, *Electrochimica Acta*, **51**, 3316 (2006).
- H. Yano, T. Tanaka, M. Nakayama, and K. Ogura, *Journal of Electroanalytical Chemistry*, **565**, 287 (2004).
- J. Yano, T. Morita, K. Shimano, Y. Nagami, and S. Yamasaki, *Journal of Solid State Electrochemistry*, **11**, 554 (2006).
- K. Ogura, *Journal of CO₂ Utilization*, **1**, 43 (2013).
- I. Ganesh, *Renewable and Sustainable Energy Reviews*, **31**, 221 (2014).
- D. P. Summers, S. Leach, and K. W. Frese Jr, *Journal of Electroanalytical Chemistry and Interfacial Electrochemistry*, **205**, 219 (1986).
- F. Jia, X. Yu, and L. Zhang, *Journal of Power Sources*, **252**, 85 (2014).
- Y. Hori, in *Modern Aspects of Electrochemistry*, eds. C. Vayenas, R. White, and M. Gamboa-Aldeco, Springer New York, 2008, Vol. 42, Ch. 3, pp. 89–189.
- M. Azuma, K. Hashimoto, M. Hiramoto, M. Watanabe, and T. Sakata, *Journal of The Electrochemical Society*, **137**, 1772 (1990).
- M. Jitaru, D. A. Lowy, M. Toma, B. C. Toma, and L. Oniciu, *Journal of Applied Electrochemistry*, **27**, 875 (1997).
- Y. Chen and M. W. Kanan, *Journal of the American Chemical Society*, **134**, 1986 (2012).
- R. Hinogami, S. Yotsuhashi, M. Deguchi, Y. Zenitani, H. Hashiba, and Y. Yamada, *ECSS Electrochemistry Letters*, **1**, H17 (2012).
- C. E. Tomow, M. R. Thorson, S. Ma, A. A. Gewirth, and P. J. A. Kenis, *Journal of the American Chemical Society*, **134**, 19520 (2012).
- H.-R. M. Jhong, S. Ma, and P. J. A. Kenis, *Current Opinion in Chemical Engineering*, **2**, 191 (2013).
- R. J. Lim, M. Xie, M. A. Sk, J.-M. Lee, A. Fisher, X. Wang, and K. H. Lim, *Catalysis Today*, 2013.
- Y. Hori, in *Handbook of Fuel Cells*, John Wiley & Sons, Ltd, 2010.
- H. Li and C. Oloman, *Journal of Applied Electrochemistry*, **37**, 1107 (2007).
- C. Delacourt, P. L. Ridgway, and J. Newman, *Journal of The Electrochemical Society*, **157**, B1902 (2010).
- M. Ni, *Journal of Power Sources*, **202**, 209 (2012).
- M. Ni, *International Journal of Hydrogen Energy*, **37**, 6389 (2012).
- Y. Xie and X. Xue, *Solid State Ionics*, **224**, 64 (2012).
- Y. Luo, Y. Shi, W. Li, and N. Cai, *Energy*, **70**, 420 (2014).
- H. Wang, D. Y. C. Leung, and J. Xuan, *Applied Energy*, **102**, 1057 (2013).
- J. van de Loosdrecht, F. G. Botes, I. M. Ciobica, A. Ferreira, P. Gibson, D. J. Moodley, A. M. Saib, J. L. Visagie, C. J. Weststrate, and J. W. Niemantsverdriet, in *Comprehensive Inorganic Chemistry II (Second Edition)*, eds. J. Reedijk and K. Poeppelmeier, Elsevier, Amsterdam, 2013, pp. 525–557.
- M. E. Dry, *Catalysis Today*, **71**, 227 (2002).
- A. P. Steynberg, in *Studies in Surface Science and Catalysis*, eds. S. André and D. Mark, Elsevier, 2004, Volume 152, pp. 1–63.
- S. Um, C. Y. Wang, and K. S. Chen, *Journal of The Electrochemical Society*, **147**, 4485 (2000).
- E. Birgersson, M. Noponen, and M. Vynnycky, *Journal of The Electrochemical Society*, **152**, A1021 (2005).
- B. Zhang, D.-d. Ye, P.-C. Sui, N. Djilali, and X. Zhu, *Journal of Power Sources*, **259**, 15 (2014).
- D. Krishnamurthy, E. O. Johansson, J. W. Lee, and E. Kjeang, *Journal of Power Sources*, **196**, 10019 (2011).
- A. Ebrahimi Khabbazi, A. J. Richards, and M. Hoorfar, *Journal of Power Sources*, **195**, 8141 (2010).
- E. U. Ubong, Z. Shi, and X. Wang, *Journal of The Electrochemical Society*, **156**, B1276 (2009).
- C. F. Curtiss and R. B. Bird, *Industrial & Engineering Chemistry Research*, **38**, 2515 (1999).
- E. L. Cussler, *Multicomponent Diffusion*, Elsevier Scientific Publishing Company, 1976.
- E. L. Cussler, *Diffusion: Mass Transfer in Fluid Systems*, Cambridge University Press, 2009.
- E. N. Fuller, P. D. Schettler, and J. C. Giddings, *Industrial & Engineering Chemistry*, **58**, 18 (1966).
- M. M. Tomadakis, *Journal of Composite Materials*, **39**, 163 (2005).
- H. R. Jhong, F. R. Brushett, L. Yin, D. M. Stevenson, and P. J. A. Kenis, *Journal of the Electrochemical Society*, **159**, B292 (2012).
- L. Ma, D. B. Ingham, and M. C. Pourkashanian, in *Transport Phenomena in Porous Media III*, eds. D. B. Ingham and I. Pop, Pergamon, Oxford, 2005, pp. 418–440.
- D. T. Whipple and D. T. PhD, University of Illinois at Urbana-Champaign, 2011.
- M. Björkman and K. Holmström *Advanced Modeling and Optimization*, **1**, (1999).
- D. Jones in *Encyclopedia of Optimization*, eds. C. A. Floudas and P. M. Pardalos, Springer US, 2009, ch. 128, pp. 725–735.
- J. R. Welty, C. E. Wicks, G. Rorrer, and R. E. Wilson, *Fundamentals of momentum, heat, and mass transfer*, John Wiley & Sons, 2009.
- J. Newman and K. E. Thomas-Alyea, *Electrochemical Systems*, 2004.
- R. H. Perry and D. W. Green, *Perry's chemical engineers' handbook*, McGraw-Hill, New York, 2008.



Erratum: Modeling and Experimental Validation of Electrochemical Reduction of CO₂ to CO in a Microfluidic Cell [J. Electrochem. Soc., 162, F23 (2015)]

Kunna Wu,^{a,b} Erik Birgersson,^a Byoungsu Kim,^b Paul J. A. Kenis,^b and Iftekhar A. Karimi^a

^aDepartment of Chemical and Biomolecular Engineering, National University of Singapore, Singapore 117585

^bDepartment of Chemical and Biomolecular Engineering, University of Illinois at Urbana-Champaign, Urbana, Illinois 61801, USA

© 2014 The Electrochemical Society. [DOI: 10.1149/2.0341503jes] All rights reserved. Published December 12, 2014.

On page F28, left column, Figure 2 should be

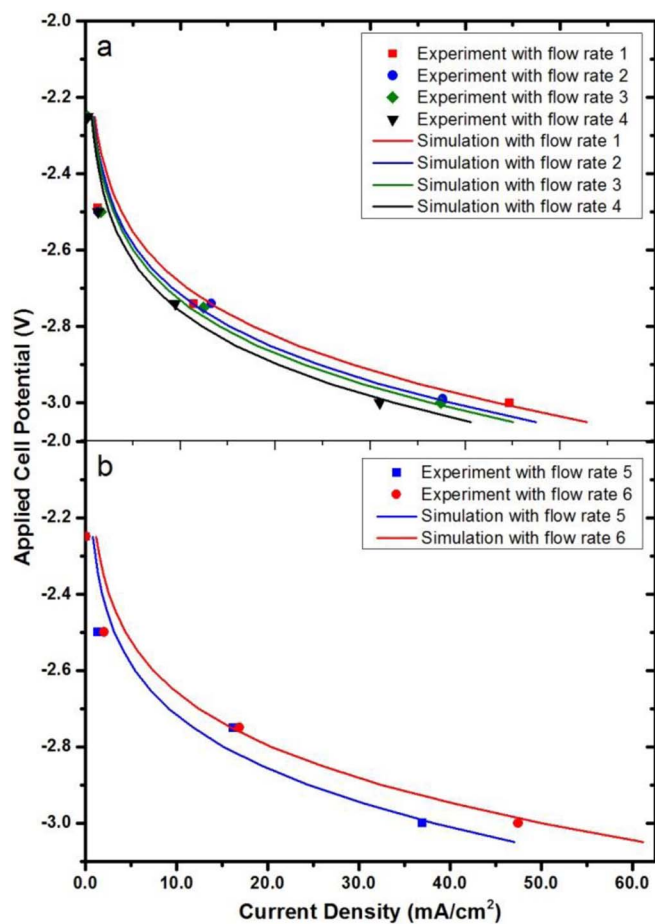


Figure 2. Comparison of polarization curves for (a) parameter fitting and (b) model validation. Feed gas flow rate and compositions are specified in Table 2. Other operating conditions take the base case values in Table 1.